Effect of the Drake Passage Throughflow on Global Climate

WILLEM P. SIJP AND MATTHEW H. ENGLAND

Centre for Environmental Modelling and Prediction, School of Mathematics, University of New South Wales, Sydney, New South Wales, Australia

(Manuscript received 15 November 2002, in final form 6 October 2003)

ABSTRACT

The role of the Southern Ocean in global climate is examined using three simulations with a coupled model employing geometries different only at the location of Drake Passage (DP). The results of three main experiments are examined: 1) a simulation with DP closed, 2) an experiment with DP at a shallow (690 m) depth, and 3) a realistic DP experiment. The climate with DP closed is characterized by warmer Southern Hemisphere surface air temperature (SAT), little Antarctic ice, and no North Atlantic Deep Water (NADW) overturn. On opening the DP to a shallow depth of 690 m there is an increase in Antarctic sea ice and a cooling of the Southern Hemisphere but still no North Atlantic overturn. On fully opening the DP, the climate is mostly similar in the Southern Hemisphere to DP at 690 m, but the model now simulates NADW formation and a warming in the Northern Hemisphere. This suggests the North Atlantic thermohaline circulation depends not only on the existence of a DP throughflow, but also on the depth of the sills in the Southern Ocean. The closed DP experiment exhibits a large amount of deep-water formation [57 Sv (Sv $\equiv 10^6$ m^3 s^{-1})] in the Southern Hemisphere; this reduces to 39 Sv for the shallow DP case and 14 Sv when DP is at 2316 m, its modern-day depth. NADW formation is shut down in both DP closed and shallow experiments, which accounts for the warming in the Northern Hemisphere observed when the DP is opened. SAT differences between the DP open and closed climate are seasonal. The largest SAT changes occur during winter in areas of large sea ice change. However, summer conditions are still significantly warmer when DP is closed (regionally up to 4°C). Summer SAT is the most important factor determining whether an Antarctic ice sheet can build up. Therefore our study does not exclude the possibility that changes in ocean gateways may have contributed to the glaciation of Antarctica. Overall, these experimental results support paleoclimatic evidence of rapid cooling of the Southern Ocean region soon after the isolation of Antarctica.

1. Introduction

The Tertiary (65 Myr ago to present) has witnessed a long cooling trend that culminated in the current climate characterized by the presence of permanent ice and periods of increased glaciation interspersed with warmer periods (interglacials) such as the present climate. This global temperature trend is not a gradual process but is characterized by distinct cooling events (Kennett 1977). One geographic shift that might have caused a Tertiary cooling event is the opening of Drake Passage (DP). This idea was first put forward by Kennett (1977), though for the land mass formed by the combination of Australia and Antarctica rather than Drake Passage itself. It is estimated (Barker and Burrell 1977) that Drake Passage opened about 30 Myr ago. It is changes in ocean gateways like this that are most likely to cause major changes in ocean circulation and thus patterns of poleward heat transport and climate.

The current study aims to examine the effects on global climate of the isolation of Antarctica behind a longitudinally uninterrupted mass of ocean water. We do not attempt to directly simulate an Oligocene or Eocene climate by using realistic topography and bathymetry reconstructions for these epochs. Rather, we simply introduce changes in landmass geography at the location of Drake Passage: all other model features are controlled at a present day scenario [e.g., carbon dioxide (CO_2) levels, solar insolation, other continental outlines, and so on]. Changes due to differing continental distributions (and thus albedos), orography, and the existence of ocean gateways and seas such as the Isthmus of Panama and the Tethys are thus beyond the scope of this study.

The role of Drake Passage in causing fundamental changes to the global thermohaline circulation (THC) has been examined in a number of previous ocean-only experiments without atmospheric feedbacks. The first modeling study to examine the Drake Passage effect was undertaken by Gill and Bryan (1971), who found increased outflow of Antarctic Bottom Water (AABW) for an idealized basin model with a closed Drake Passage. Later studies incorporated a global domain, but still no atmospheric or sea ice effects. For example, Cox

Corresponding author address: Willem P. Sijp, Centre for Environmental Modelling and Prediction, School of Mathematics, University of New South Wales, Sydney NSW 2052, Australia.
E-mail: wsijp@maths.unsw.edu.au

(1989), England (1992), and Toggweiler and Samuels (1995) note the absence of any north–south geostrophic flow in the zonally unbounded region of the Southern Ocean. This means northward surface Ekman transport under the subpolar westerlies must be balanced by a deeper return flow (Toggweiler and Samuels 1995), though this relation appears to weaken when ocean–atmosphere thermal feedback is allowed (Rahmstorf and England 1997). The effects of ocean gateway configurations on heat fluxes and surface air temperatures were studied by Mikolajewicz et al. (1993) using an ocean-only model employing mixed boundary conditions in experiments including Drake Passage closed/open and Isthmus of Panama closed/open. Their study indicated a 0.8°C cooling (zonally averaged) at 50°S upon opening Drake Passage, a result of compensating areas of warming and cooling in the Southern Hemisphere (SH).

The models used in the above studies were all ocean-only models, namely, without an interactive atmospheric model. With such a fundamental shift in model geometry as opening and closing DP, a coupled model is needed to incorporate possible feedbacks between the ocean, atmosphere, and sea ice. One study of the DP effect in a model including some atmospheric processes is that of Nong et al. (2000). They use a realistic topography ocean model with an atmospheric heat diffusion parameterization; however, they restore to fixed zonally averaged salinities. They find a substantial atmospheric cooling in the Southern Hemisphere and colder deep waters upon opening DP. They also obtain North Atlantic Deep Water (NADW) formation when DP is closed, though this is likely to be an artifact of suppressing a free response to changes in oceanic salinity transport by restoring to modern day sea surface salinities. In addition, Nong et al. (2000) incorporate no sea ice and no seasonality, which will underestimate SAT changes due to the opening of DP.

Toggweiler and Bjornsson (2000) conducted a study using a simplified coupled ocean–atmosphere model with idealized bathymetry (a water planet model) using the Geophysical Fluid Dynamics Laboratory (GFDL) Modular Ocean Model (MOM) with wind and salinity forcing symmetrical about the equator. The atmospheric component solves a one-dimensional equation describing the latitudinal variation of the atmospheric heat budget. There are no restoring boundary conditions for heat transfer between the ocean and atmosphere. However, this model includes no ice, hydrological cycle, or interactive winds. Toggweiler and Bjornsson (2000) found air and sea temperatures to be around 3°C cooler at high southern latitudes when Drake Passage is opened. He also analyzes a shallow DP experiment and concludes that the global thermal response to the opening of Drake Passage could have been abrupt.

Other previous coupled model studies of the DP effect are those of Bryan et al. (1988), Huber et al. (2003), and Huber and Nof (2003, manuscript submitted to *Geophys. Monogr.,* hereinafter HN). Bryan et al. (1988) conducted DP closed experiments under climate change scenarios with a full coupled model but a simplified sector geometry. They found no NADW and a large [55 Sv (Sv $\equiv 10^6$ m^3 s^{-1})] overturning cell adjacent to Antarctica when DP is closed. The goal of their study was to examine the relative role of the Drake Passage effect (and associated subduction) versus the large ratio of ocean to land in the Southern Hemisphere as a mechanism for retarding air temperature change. Huber et al. (2003) and HN study the possible relation among Eocene–Oligocene climate deterioration, Southern Ocean gateway changes, and atmospheric CO_2 concentrations using a coupled model with realistic geometry. They find that climate change in these past epochs was most likely due to the influence of greenhouse gases. In our study, the focus is on mechanisms driving fundamental changes in circulation and climate and the particular role of the DP gap. No formal paleoclimate reconstruction is attempted.

The rest of this paper is divided as follows. Section 2 consists of a description of the model and experimental design. In section 3 we examine changes in sea surface temperature (SST) and the global ocean circulation resulting from DP opening. Meridional overturning (MOT) changes are compared with those found in previous studies with ocean-only models. Sea surface currents and the barotropic streamfunction are examined and the planetary poleward heat transport is also calculated. In section 4 the sea ice response to these changes in ocean currents and heat transport is examined. Surface air temperature (SAT) changes are examined in section 5. Section 6 covers an analysis of our results in the context of previous studies. Last, section 7 covers the discussion and conclusions.

2. Model description and experimental design

a. The model

The simulations have been carried out using the Earth System Climate Model of intermediate complexity of Weaver et al. (2001). The model comprises an ocean general circulation model coupled to an atmospheric model. A hydrological cycle with river basins configured over a realistic geometry and a dynamic/thermodynamic sea ice model are included. All components of the model have a global domain with horizontal resolution 3.6° longitude by 1.8° latitude. There are 19 vertical levels in the ocean and no layering in the sea ice model.

The ocean component of the coupled model is the GFDL Modular Ocean Model (Pacanowski 1995). MOM is based on the Navier–Stokes equations subject to the Boussinesq and hydrostatic approximations. We employ constant horizontal diffusivity of 2.0×10^7 cm^2 s^{-1}, horizontal viscosity of 2.0×10^9 cm^2 s^{-1}, and vertical viscosity of 10 cm^2 s^{-1}. Vertical mixing is achieved through a modified form of the Bryan and Lewis (1979) vertical distribution, ranging from $k_v =$

0.6 $cm^2\ s^{-1}$ in the upper ocean to $k_v = 1.6\ cm^2\ s^{-1}$ in the deep ocean. There is also a parameterization of brine rejection during sea ice formation (after Duffy and Caldeira 1997). Surface forcing is accomplished using wind stresses calculated from wind fields in the atmospheric component, and ice–air–sea heat and freshwater fluxes.

The atmospheric model consists of a 2D energy balance model based on Fanning and Weaver (1996). The model has one vertical layer. The model allows for redistribution of thermal energy and moisture content through a single vertically integrated equation for each. Moisture transports are accomplished through advection (by wind) and Fickian diffusion. Wind fields act on the ocean through the calculation of a wind stress. Wind also influences evaporation rates, heat fluxes to the ocean, and moisture advection. Precipitation is assumed to occur when relative humidity is greater than 85%. Precipitation that falls over land is returned to the ocean instantaneously via prescribed river basins.

The wind field is not determined exclusively by prognostic equations for momentum conservation, but are based on specific wind data taken from National Centers of Environmental Prediction (NCEP)–National Center for Atmospheric Research (NCAR) reanalysis (Kalnay et al. 1996), averaged over the period 1958–97 to form an annual cycle from the monthly fields. A dynamical wind feedback is included in the form of a term that indicates departure from the mean field. Wind feedbacks are calculated from temperature changes from a mean climatology using a latitudinally dependent relationship between temperature and air density. Transport of heat is not accomplished through advection, only through Fickian diffusion. Indirectly, advective heat transport can occur through the transport of moisture in the atmosphere and consequent precipitation whereby latent heat is released. Model atmospheric temperatures decrease over uplifted land areas according to a fixed lapse rate.

The energy conserving thermodynamic sea ice model predicts ice thickness, areal fraction, and ice surface temperature. Sea ice dynamics are achieved by an elastic–viscous–plastic representation (Hunke and Dukowicz 1997). The subgrid-scale ice thickness distribution allows for two ice categories within each model grid cell.

Precipitation creates snow cover when the SAT drops below -5°C. Both snow and sea ice influence planetary albedo. Surface specific humidity changes at a given location are fully determined by the vertically integrated atmospheric moisture balance equation that includes an advection term and a Fickian diffusion term with a constant eddy diffusivity coefficient of $10^6\ m^2\ s^{-1}$ (see Weaver et al. 2001).

b. Experimental design

Our study is based on three main experiments, set up identically with the exception of bathymetry. The first experiment (DP_{clsd}, is conducted with a bathymetry where DP is closed by a land bridge between the Antarctic Peninsula and South America. The second experiment employs a bathymetry with DP open to a maximum depth of 690 m (denoted DP_{690}). In the third experiment (denoted DP_{open}), DP is open at its present day depth, which is modeled as an uninterrupted throughflow at depth 2316 m. Other auxiliary experiments are also conducted, including one with DP open to 1386 m (DP_{1386}) as well as a repeat of the three main experiments with different mixing parameterizations [including using Gent and McWilliams (1990) eddy advection]. This latter set of experiments was designed to test robustness of results to subgrid-scale mixing.

The three main experiments involve running the model for 4500 years from idealized initial conditions. This procedure yields a stable model climate with very small variability and no observable drift in the thermohaline properties of the circulation field. Annual-mean meridional overturning rates vary by no more than 0.5 Sv at this stage of the model integration. In a future paper, we explore the sensitivity of these final model climate states to perturbations in high-latitude freshwater forcing. For the present, our focus is on the equilibrated solutions. All properties used in this paper are derived from averages over 100 years of integration at the end of the 4500-year integration. The model runs include atmospheric wind and thermal feedbacks and moisture advection.

3. Ocean circulation response

a. Meridional overturning

Meridional overturning is shown for experiments DP_{clsd}, DP_{690}, and DP_{open} in Fig. 1. Table 1 shows MOT in the Northern and Southern Hemisphere for DP_{clsd}, DP_{690}, DP_{1386}, and DP_{open} measured by the maximum value of the zonally averaged streamfunction at latitudes of deepwater formation. The DP_{clsd} experiment exhibits 57 Sv of sinking next to Antarctica, whereas the DP_{690} case has only 39 Sv. In the DP_{clsd}, DP_{690}, and DP_{1386} cases the meridional overturning cell in the Northern Hemisphere (NH) related to the formation of NADW is absent. In contrast, the DP_{open} experiment exhibits a Northern Hemisphere sinking of 21 Sv. In addition, AABW formation in DP_{open} is further reduced to 14 Sv. This underscores the shift of southern to northern sinking of deep water as DP is opened and deepened.

The Deacon cell is very shallow for the DP_{clsd} case (extending to 500 m), becomes deeper in the DP_{690} experiment (extending to 1200 m), and extends to almost 3000 m depth in the DP_{open} experiment. These overturning results are qualitatively similar to those of Mikolajewicz et al. (1993) and other ocean-only model studies (e.g., England 1992). Abyssal upwelling rates of water of southern origin differ markedly between the experiments. For example, about 30 Sv of southern deep

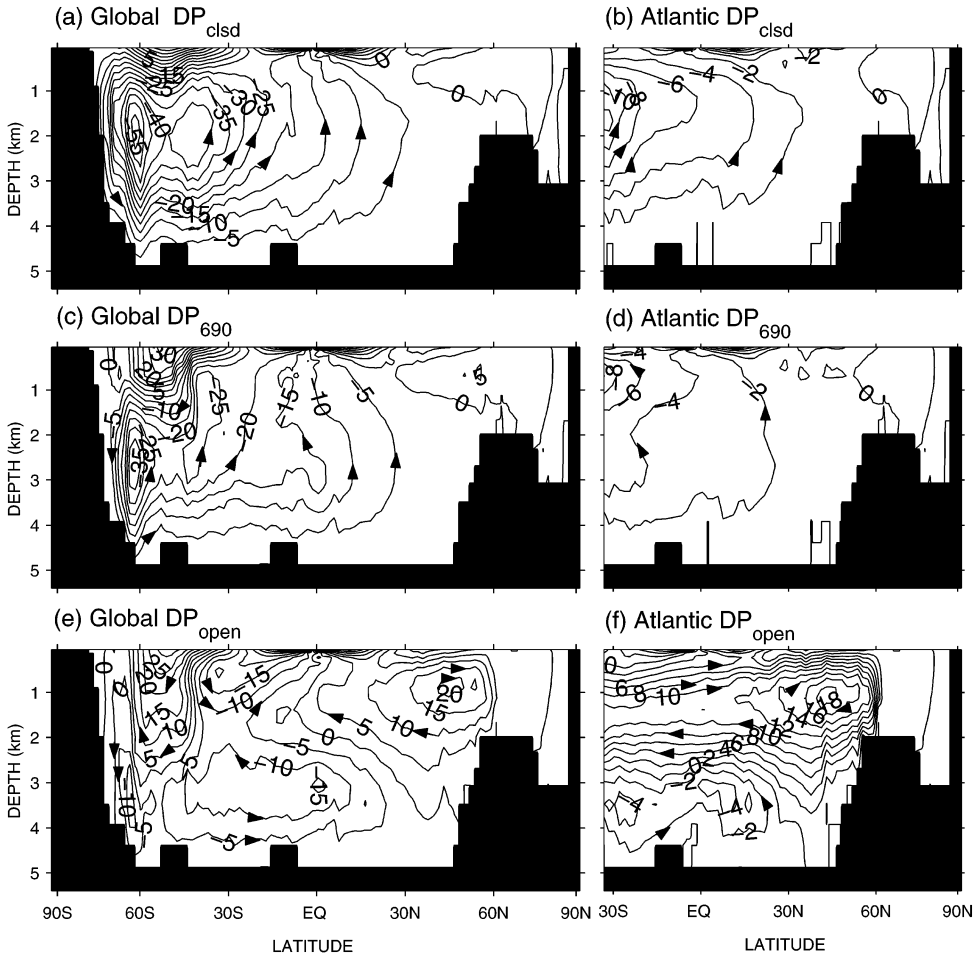

FIG. 1. (left) Global and (right) Atlantic meridional overturning streamfunction (annual average; Sv) for (a), (b) the DP_{clsd} case, (c), (d) the DP_{690} case, and (e), (f) the DP_{open} case.

water upwells across 2000 m between 30°S and 30°N in the DP_{clsd} experiment. This upwelling is only 20 Sv in the DP_{690} case, and order 5 Sv in DP_{open}. Clearly AABW ventilation effects diminish as DP is opened and deepened.

b. Interior ocean temperature

Figure 2 shows the zonal mean sea temperature difference for $DP_{690} - DP_{clsd}$ and $DP_{open} - DP_{clsd}$. Upon opening DP to a shallow depth, upper-ocean Southern Hemisphere zonal mean cooling is of the order of 0.5°–1°C south of 30°S. An area of warming (up to 1.5°–2°C zonal mean) is observed around 1000-m depth at low latitudes caused by reduced abyssal upwelling across 2000-m depth in this region. Further reduction of abyssal upwelling combined with the establishment of NADW formation result in a significantly larger and more intense area of middepth warming (up to 2.5°C) in the DP_{open} experiment. Significant cooling of up to 2°C in the zonal mean is also present above 1000-m depth and south of 30°S in the DP_{open} experiment.

TABLE 1. Maximum MOT in the Northern and Southern Hemisphere for DP_{clsd}, DP_{690}, DP_{1386}, and DP_{open} measured by the maximum value of the zonally averaged streamfunction at latitudes of deep-water formation. Mass transport (Sv) for the Antarctic Circumpolar Current, the Brazil Current, and the Gulf Stream is also displayed.

Expt	SH MOT	NH MOT	ACC	Brazil Current	Gulf Stream
DP_{clsd}	57	4	—	66	24
DP_{690}	39	5	64	47	24
DP_{1386}	21	6	121	25	24
DP_{open}	14	21	127	21	44

c. Horizontal ocean streamfunction

Figure 3 shows the barotropic streamfunction for our three model experiments, as well as the streamfunction difference for $DP_{open} - DP_{clsd}$. Also, Table 1 shows mass transport for the Antarctic Circumpolar Current, the Brazil Current, and the Gulf Stream. Changes in the horizontal ocean circulation are limited to the Southern Ocean and the North Atlantic. Figure 3a shows that

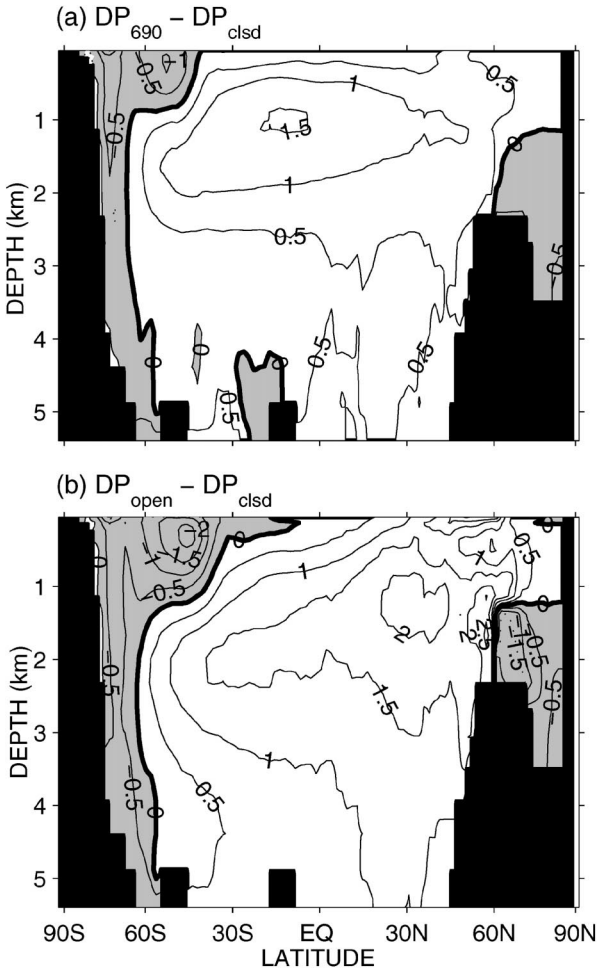

FIG. 2. Zonal mean of ocean temperature difference (year average; °C) for (a) $DP_{open} - DP_{clsd}$ and (b) $DP_{690} - DP_{clsd}$. Shaded areas denote regions of negative temperature differences.

geostrophic currents are possible across the closed DP. This means a stronger Brazil Current that, along with a weaker Gulf Stream, gives an increase of oceanic heat transport from the equator to high southern latitudes when DP is closed. A large anticyclonic gyre spanning the South Atlantic and the southern Indian Ocean of order 50 Sv exists in the DP_{clsd} experiment. This suggests a substantial Indian to Atlantic ''Agulhas leakage'' when the DP is closed. Figure 3b shows that a strong Agulhas leakage also exists in the DP_{690} experiment, but is weaker (order 20 Sv) and does not extend as far south. In DP_{open} the near absence of the Agulhas leakage (around 3 Sv) cools the eastern section of the South Atlantic. The ACC has a strength of 64 Sv in DP_{690} increasing to 127 Sv in DP_{open} (Table 1). Note the small difference in ACC transport between DP_{open} and DP_{1386} in Table 1, indicating most transport in the ACC appears in the upper 1500 m of the model.

The Indonesian Throughflow has values between 24 and 28 Sv in all three experiments. In the DP_{clsd} experiment a cyclonic polar gyre of about 60 Sv is present in the Ross Sea, indicating an increased east-wind drift in this region. This gyre is contained in a larger gyre of about 10 Sv that spans the latitudes of DP from west of the Antarctic Peninsula eastward to the Weddell Sea, indicating a general increase in the east wind drift around Antarctica when DP is closed.

The differenced streamfunction ($DP_{open} - DP_{clsd}$) shows the ACC as the principal change in horizontal ocean circulation between the fully opened and closed DP experiments. Also shown is a reduction in the three Southern Hemisphere western boundary currents. Most notable, mass transport in the Brazil Current is reduced from 66 to 21 Sv when DP is opened (see Table 1). North Atlantic circulation changes include the strengthening of the Labrador Current when DP is opened and an increase of 20 Sv in the Gulf Stream. This near doubling of the Gulf Stream is almost entirely due to the establishment of NADW formation in DP_{open}. This is discussed further in section 6.

d. Sea surface temperatures and ocean currents

Figure 4 shows global SST and current differences between DP_{690} and DP_{clsd}, and between DP_{open} and DP_{clsd}. Differences in North Atlantic SST and flow are negligible between DP_{690} and DP_{clsd}. SST in the North Atlantic for DP_{open} is up to 6°–7°C warmer than in DP_{clsd} because of the establishment of deep-water formation in this region. Figure 4b shows that the increased Gulf Stream in DP_{open} transports warmer waters to the North Atlantic from lower latitudes.

When DP is opened to 690-m depth, the Brazil Current decreases in strength because of the absence of a western boundary connecting Antarctica and South America, and the Agulhas current no longer flows into the South Atlantic. This results in an area of cooling of up to 10°C observed for DP_{690} at southern midlatitudes in the west of the Atlantic. Also, DP_{open} exhibits an area with similar values of cooling (up to 10°C) that extends farther east into the Indian Ocean. SST changes west of the Antarctic Peninsula are similar in both the DP_{690} experiment and DP_{open} experiment with a cooling of around 4°C.

The ACC (absent in DP_{clsd}) flows in a southeasterly direction in the Indian Ocean, bringing warmer waters south in the DP_{open} experiment. This results in a warming of 4°C south of Australia for the DP_{open} experiment, with a smaller area of warming of similar magnitude in the DP_{690} experiment. Figure 4b shows that the Southern Hemisphere area of warming coincides with the area where a southeastward current is established. Overall, the similarity of SST changes in the Southern Hemisphere in Figs. 4a and 4b suggests that a southern cooling occurred soon after the isolation of Antarctica.

e. Poleward heat transport

Figure 5 shows the northward oceanic heat transport for DP_{clsd} (blue), DP_{690} (black), and DP_{open} (green). There

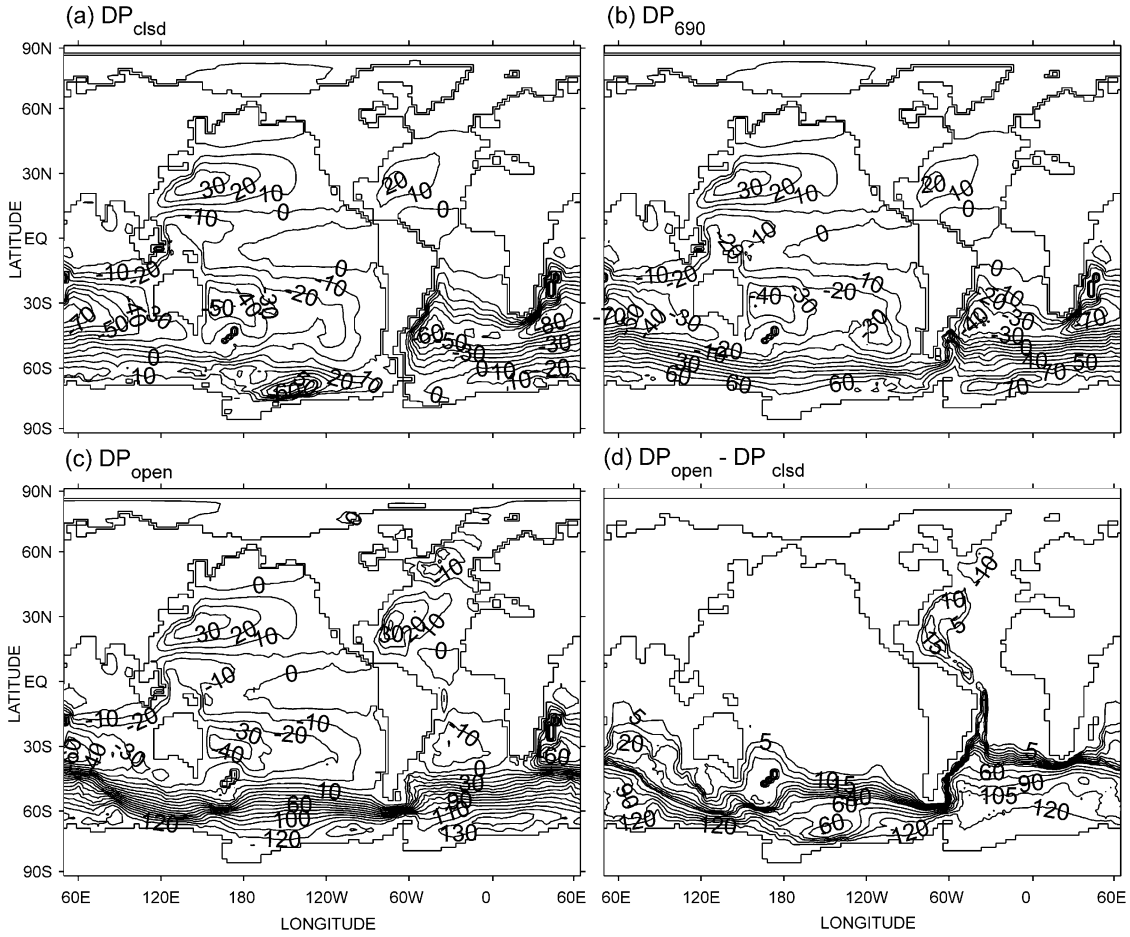

FIG. 3. Annual average (Sv) of the ocean barotropic streamfunction for (a) DP_{clsd}, (b) DP_{690}, and (c) DP_{open} experiments and (d) the barotropic streamfunction difference for $DP_{open} - DP_{clsd}$.

is a decrease of maximum southward oceanic heat transport at low latitudes in the Southern Hemisphere from 2.3 PW (DP_{clsd}) to 2.1 PW (DP_{690}) when opening DP to a shallow depth. Northern Hemisphere oceanic heat transport is virtually the same for DP_{clsd} and DP_{690} (maximum of order 0.6 PW). Changes in poleward heat transport in these experiments can be directly related to changes in the ocean's MOT. For example, the decrease in Southern Hemisphere heat transport in DP_{690} is caused by the decrease in southern MOT (Fig. 1). Similarly, with little change in NADW between DP_{clsd} and DP_{690}, little difference is seen in Northern Hemisphere heat transport in those runs.

There is a decrease of southward oceanic heat transport at low latitudes in the Southern Hemisphere from 2.3 (DP_{clsd}) to 1.8 PW (DP_{open}) when opening DP to full depth. This decrease is larger than in DP_{690} and is caused by a larger reduction in Southern Hemisphere MOT (Fig. 1) for DP_{open}. Increased NADW formation in DP_{open} also contributes to a decrease in Southern Hemisphere MOT and poleward heat transport. Northern Hemisphere heat transport at low latitudes increases from 0.6 (DP_{clsd}) to 1.2 PW (DP_{open}) when DP is opened to full depth. This increase is caused by the initiation of NADW formation in the DP_{open} experiment. These changes in poleward heat transport between DP_{clsd} and DP_{open} are surprisingly similar in magnitude to those simulated in paleoclimate models for the Eocene by Huber et al. (2003). However, in our study we only change the DP gateway geometry and keep all other parameters constant (e.g., CO_2 levels, solar insolation). We therefore offer no direct simulations of past climate states, only indirect estimates of the possible role played by DP gateway changes.

4. Sea ice response

Figure 6 shows the annual sea ice frequencies for all three experiments, as well as the difference in annual sea ice frequency between DP_{open} and DP_{clsd}. Southern Hemisphere sea ice extent and frequency increases significantly when DP is opened to a shallow depth in DP_{690} (Fig. 6b), particularly in the region east of the the Ross Sea, which is almost ice free all year in DP_{clsd}. Com-

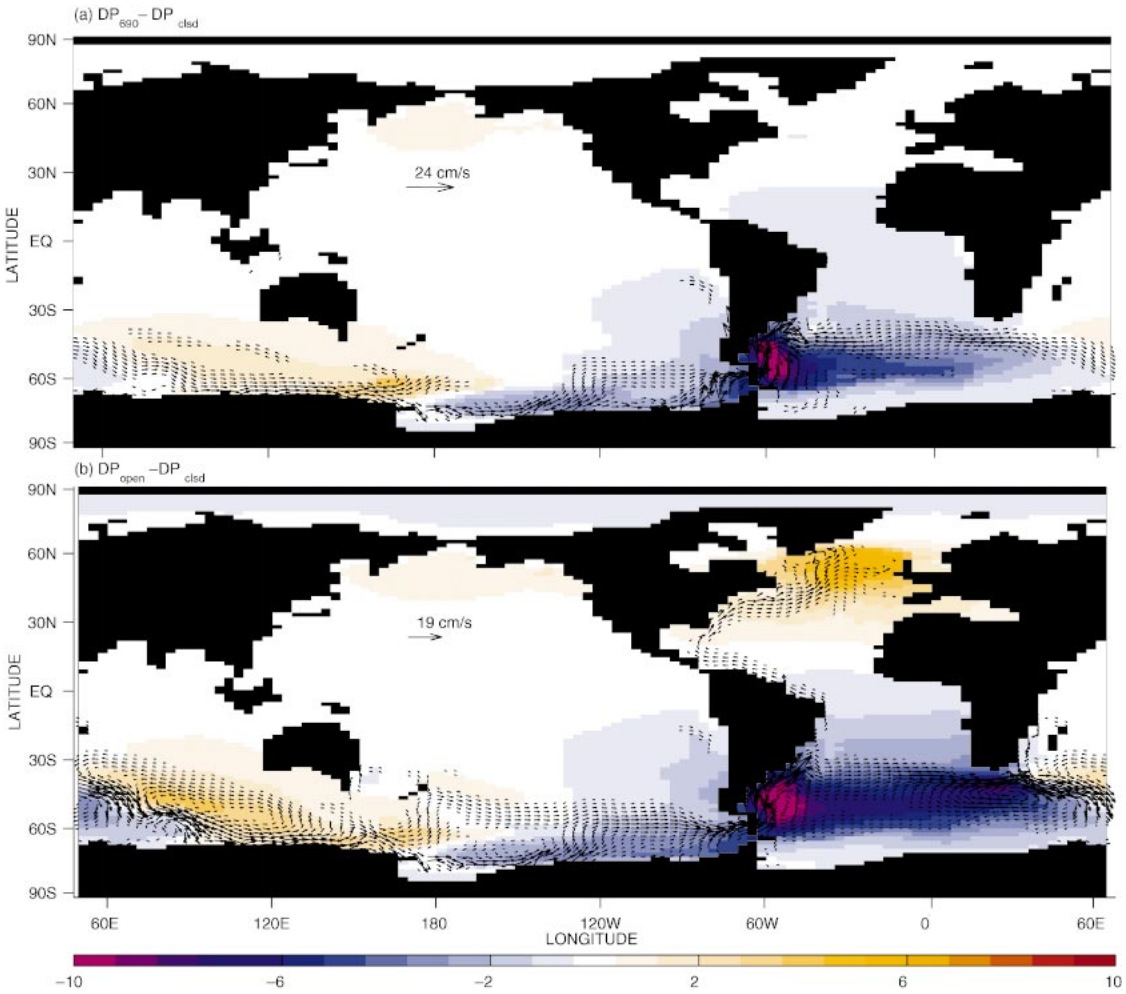

FIG. 4. Annual average of sea surface temperature difference (at 25-m depth; °C). Overlaid are vectors of ocean current differences at the surface. A vector scale is included.

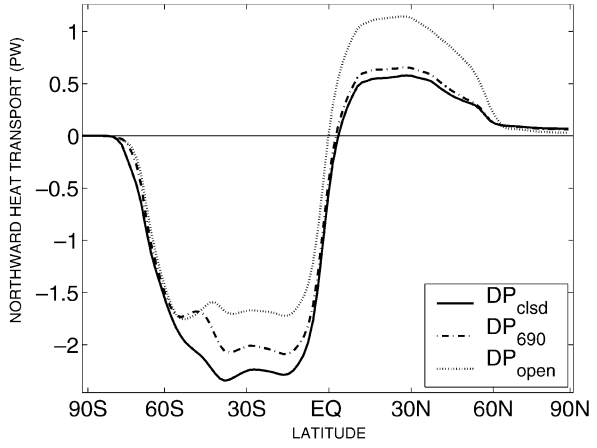

FIG. 5. Northward oceanic heat transport in DP_{clsd}, DP_{690}, and DP_{open}.

parison of Fig. 6b with Fig. 6d shows that Southern Hemisphere sea ice changes are abrupt upon opening DP with most of the changes achieved already for a shallow DP. The Southern Hemisphere sea ice increase is due to decreased southward ocean heat transport and a positive feedback when increased ice leads to increased albedo.

Figures 6b and 6d indicate that sea ice increases are most intense adjacent to the Antarctic continent between the Ross Sea and the Antarctic Peninsula. Maximum oceanic heat loss to the atmosphere is observed in this region in DP_{clsd} (not shown). An active convection scheme mixes temperature and salinity vertically over unstable portions of the water column. During winter the water column becomes unstable in isolated locations around Antarctica due to brine rejection and surface cooling. Subsequent vertical overturn brings warm deeper water to the surface, which enhances oceanic heat release and causes sea ice melt.

A decrease in sea ice west of the Ross Sea is observed

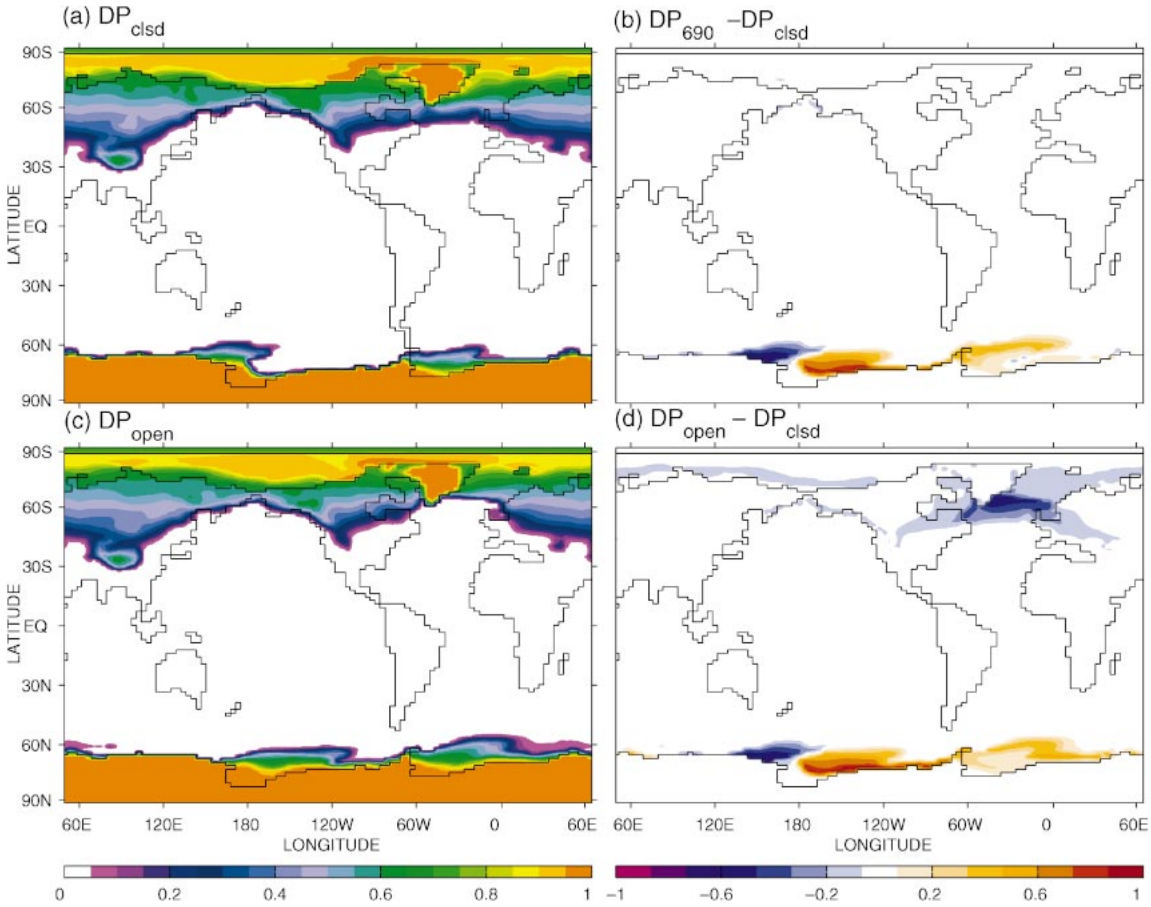

FIG. 6. Annual-mean sea ice frequencies for (a) DP_{clsd}, (b) $DP_{690} - DP_{clsd}$ (difference), (c) DP_{open}, and (d) $DP_{open} - DP_{clsd}$ (difference). [Note added in proof: The latitude labels are erroneously reversed, north to south, but the data are correct.—Ed.]

in DP_{690} and DP_{open}. In these experiments, the ACC flows southeastward in this region, forcing ice free conditions (see also Fig. 4). There are no significant changes in Northern Hemisphere sea ice distribution upon opening DP to a shallow depth in DP_{690}. In contrast, a reduction is achieved when DP is opened to its full depth as NADW formation leads to warmer northern latitudes and sea ice melt back.

5. Atmospheric response

a. Air temperatures

Figure 7 shows the change in yearly averaged surface air temperature upon opening DP to 690 m (Fig. 7a) and to full depth (Fig. 7b). The DP_{690} experiment exhibits no warming (relative to DP_{clsd}) in the Northern Hemisphere, as neither experiment exhibits NADW formation. SAT cooling of up to 6°C occurs in DP_{690} over the western region of the South Atlantic close to DP and at higher southern latitudes between the Ross Sea and the Antarctic Peninsula (where cooling is almost 8°C). The area of SAT cooling in the South Atlantic extends significantly eastward in the DP_{open} experiment (Fig. 7b) with a large area of cooling of up to 5°C extending from South America to the longitudes of Africa. The area of largest SAT cooling (up to 9°–10°C) for DP_{open} occurs at higher southern latitudes between the Ross Sea and the Antarctic Peninsula and is very similar in shape to the corresponding area in DP_{690}. This similarity between Southern Hemisphere air temperatures in DP_{690} and DP_{open} suggests that the principal climate changes occurred soon after the opening of a southern gateway.

Table 2 shows the maximum zonal mean values of SAT cooling for DP_{690} and DP_{open}. A maximum annual and zonal mean value of 2.5°C (3.7°C) cooling is obtained for DP_{690} (DP_{open}). These values are highly seasonal though, with a maximum cooling of 2.4°C in the Southern Hemisphere summer and 5.3°C in the Southern Hemisphere winter for DP_{open}.

b. Seasonal differences of air temperatures

Figures 7c and 7d show the SAT differences between the months December–February and May–July, indicating a high seasonality for atmospheric temperature

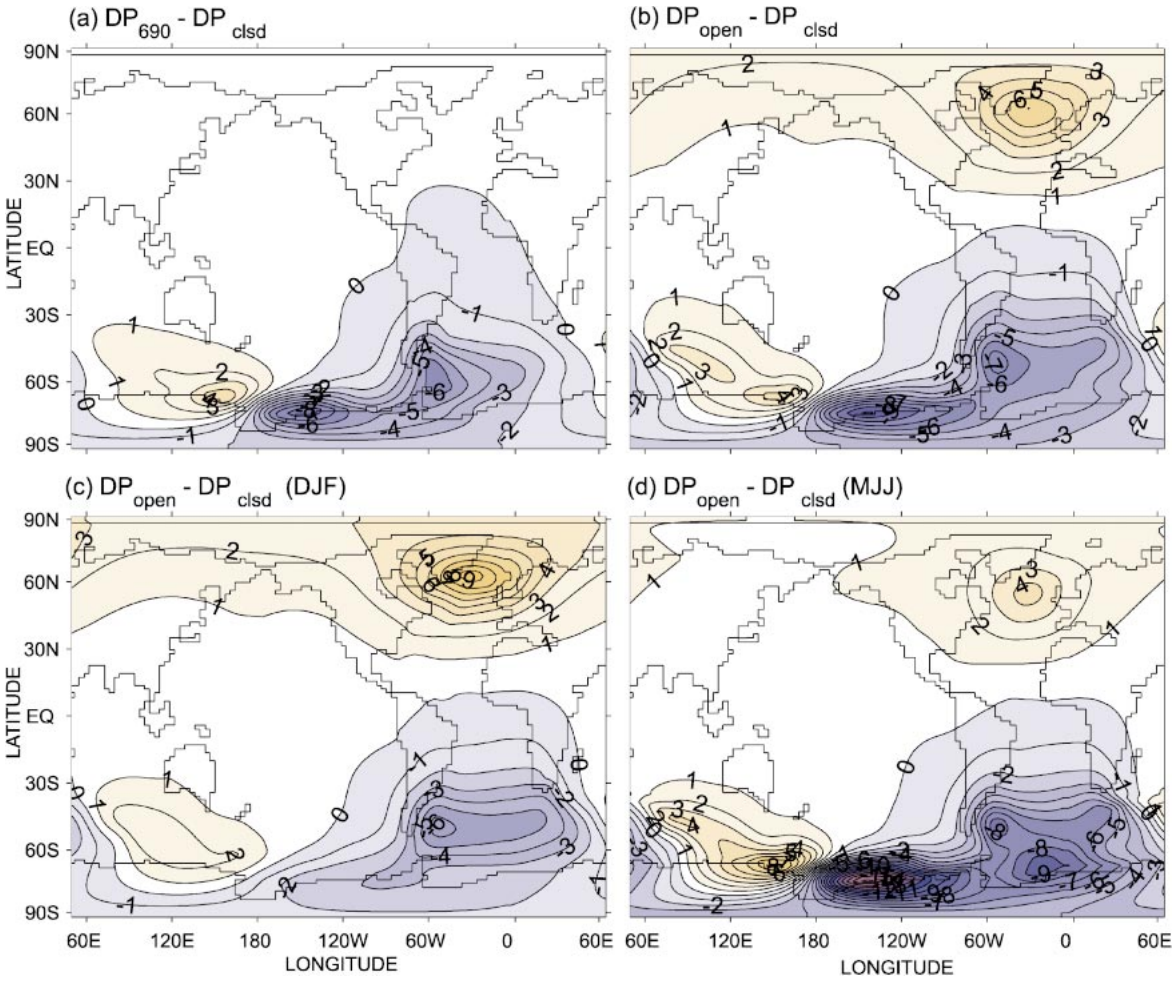

FIG. 7. Annual surface air temperature difference (°C) for (a) $DP_{690} - DP_{clsd}$ and (b) $DP_{open} - DP_{clsd}$. Seasonal surface air temperature differences (°C) for $DP_{open} - DP_{clsd}$ for (c) Dec–Feb and (d) May–Jul.

changes. Southern Hemisphere SAT changes have a much greater amplitude during winter than during summer. The same appears to hold for the North Atlantic.

The region of maximum Southern Hemisphere summertime atmospheric cooling coincides with the region of maximum SST cooling at midlatitudes in the South Atlantic (cf. Figs. 7b with Fig. 4). In summer, ocean surface temperature changes clearly control SAT change. In contrast, during the May–July period maximum SAT differences (up to 15°C) occur between the Ross Sea and the Antarctic Peninsula. This is related to regional changes in sea ice distribution caused by differences in poleward heat transport patterns, as discussed in section 4.

TABLE 2. Minima of temporal means of zonal mean SAT differences (°C) upon opening Drake Passage for DP_{690} and DP_{open}. Time periods included are the entire year, Jan–Mar, and Jul–Sep.

Expt	Annual average	Jan–Mar average	Jul–Sep average
$DP_{690} - DP_{clsd}$	−2.3	−1.6	−3.3
$DP_{open} - DP_{clsd}$	−3.7	−2.4	−5.3

6. Comparison with previous studies

In this section we make a comparison between the results of our study with previous modeling efforts to understand the role of the DP bathymetry. We can broadly classify these previous model studies according to their treatment of feedback physics in relation to the MOT. In models with an interactive atmosphere and no restoring boundary conditions for salinity, two feedbacks determine the MOT pattern (Rahmstorf and Willebrand 1995; Zang et al. 1993), namely:

1) A positive salt feedback occurs when overturning in one hemisphere gets stronger, forcing the advection of more salt from the lower latitude net evaporation zones toward the deep-water formation regions, thereby reinforcing the overturning by making the surface waters denser (provided residence times in

the higher latitude net precipitation zones are small enough). If this feedback is strong enough, it will allow the deep ocean to be filled with water that is denser than that able to be formed in the other hemisphere, suppressing deep-water formation there.

2) A negative thermal feedback exists that stabilizes the water column in deep-water formation regions when overturning is ''too large'' by allowing the increased heat transport to warm the deep-water formation areas. Conversely a weak overturning results in a lack of heat transport to the deep-water formation regions, cooling SST there and increasing the overturning rate.

Feedback 2 essentially promotes a symmetric MOT whereas feedback 1 reinforces meridional asymmetry if it is already present. Examination of previous studies of the DP effect on global ocean circulation is facilitated by classifying the models according to their representation of these two feedback processes.

a. Models without feedbacks 1 and 2

Studies employing surface restoring to observed temperature and salinity inhibit both feedbacks concurrently. Examples include England (1993), Cox (1989), and Toggweiler and Samuels (1995). Each of these studies find large overturning adjacent to Antarctica and negligible NH overturn when DP is closed. Opening DP yields a large reduction in overturn adjacent to Antarctica and NH overturn increases. Here the mode of deep-water formation is highly sensitive to the location of maximum surface-restoring density (England 1993), thus forming deep water adjacent to Antarctica for DP closed. The introduction of topographic meridional asymmetry when opening DP allows this pattern to be modified to a large degree (reducing SH overturn). These experiments illustrate how MOT symmetry is affected by topography and surface salinity forcing when feedbacks 1 and 2 are absent.

b. Models with only feedbacks 1 or 2

Models that employ restoring boundary conditions inhibit feedback 1 (when restoring salinity) or feedback 2 (when restoring temperature). The Mikolajewicz et al. (1993) model restores SST to climatological data but employs fixed surface salinity fluxes, thus allowing only feedback 1 to operate. This use of an asymmetric salinity flux forcing in the absence of a stabilizing thermal feedback allows the effect of the asymmetry to be amplified in DP closed experiments. This results in large SH overturn (90–100 Sv) which shuts down NH overturn.

Alternatively, models with an energy balance atmosphere and restoring salinity conditions, such as that of Nong et al. (2000), inhibit the positive salt feedback while allowing the thermal feedback. Nong et al. found large overturning around Antarctica, but also NH overturn for DP closed, in stark contrast to our study. MOT asymmetry is suppressed as their model allows no positive salt feedback. In addition, restoring to present-day NH surface salinities forces NH overturn to coexist with a vigorous SH overturn when the DP is closed. This result is most likely an artifact of their neglect of a free response of surface salinities to changes in oceanic salinity transport.

c. Models with both feedbacks 1 and 2

Our study and Toggweiler and Bjornsson (2000) are examples in which both feedbacks operate. In the case of Toggweiler and Bjornsson (2000), a meridionally symmetric fixed FW flux field is employed, resulting in a meridionally symmetric MOT for DP closed. By also employing an idealized meridionally symmetric topography, Toggweiler and Bjornsson (2000) focus on the asymmetry introduced to the MOT by the inhibition of SH overturn upon opening the DP gap. In the model that we use, salinity forcing is not prescribed and a meridional asymmetry develops as sea ice production around Antarctica and wind-driven advection of sea ice away from the production regions causes a significant wintertime salinity flux into the ocean through brine rejection in these areas (figure not shown).

It is of interest to diagnose the relative roles of surface freshwater (FW) fluxes versus oceanic salt transport in controlling MOT in the North Atlantic in our model experiments. Figure 8 shows the North Atlantic zonal mean of FW flux into the ocean and the corresponding zonal mean of sea surface salinity in experiments DP_{clsd} and DP_{open}. We find that the North Atlantic becomes much saltier upon opening the DP, whereas surface salinity flux changes are small and are mainly driven by the southward displacement of the sea ice edge, representing a redistribution of the FW fluxes due to sea ice melt. Therefore, in our study, the sea surface salinity changes in the NH are not the result of changes in FW forcing across the sea surface but are caused by changes in oceanic salt transport, indicating a weak feedback between oceanic circulation and the atmospheric hydrological cycle [also found in Saenko et al. (2002) and Hughes and Weaver (1994)].

The positive salt feedback is therefore an important driver for salinity distribution changes in the model. Our pattern of salinity change in the North Atlantic in DP_{clsd} is characteristic of that associated with NADW ''collapse.'' For instance, Manabe and Stouffer (1988) and Rahmstorf (1996) find similar salinity differences in the Atlantic due to a change between the ''on'' and ''off'' state of NADW formation, ascribing this to changes in oceanic salt transport. Studies that suppress the surface salinity response to such changes miss important physics in the earth's climate system. It is interesting to note that Bryan et al. (1988) find SH overturn of comparable magnitude (55 Sv) to our study and no NH overturn when DP is closed. As in our model, they employ no

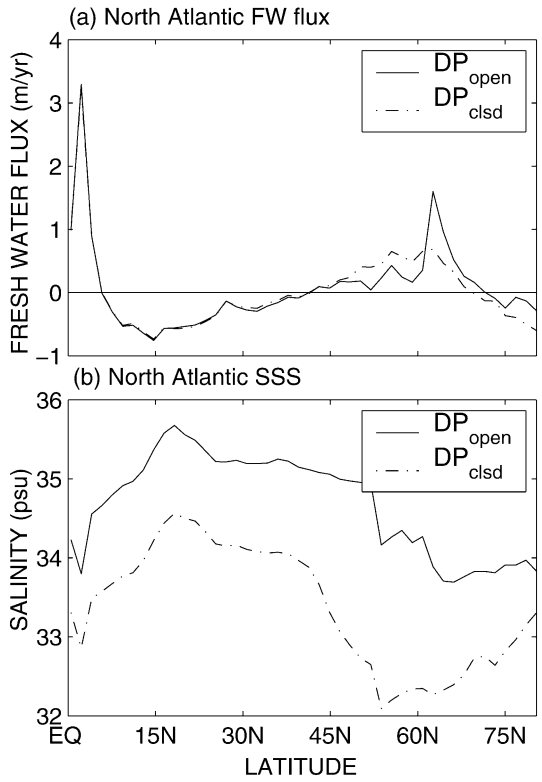

FIG. 8. (a) Zonal mean of freshwater flux into the North Atlantic and (b) zonal mean of sea surface salinity (SSS) in the North Atlantic.

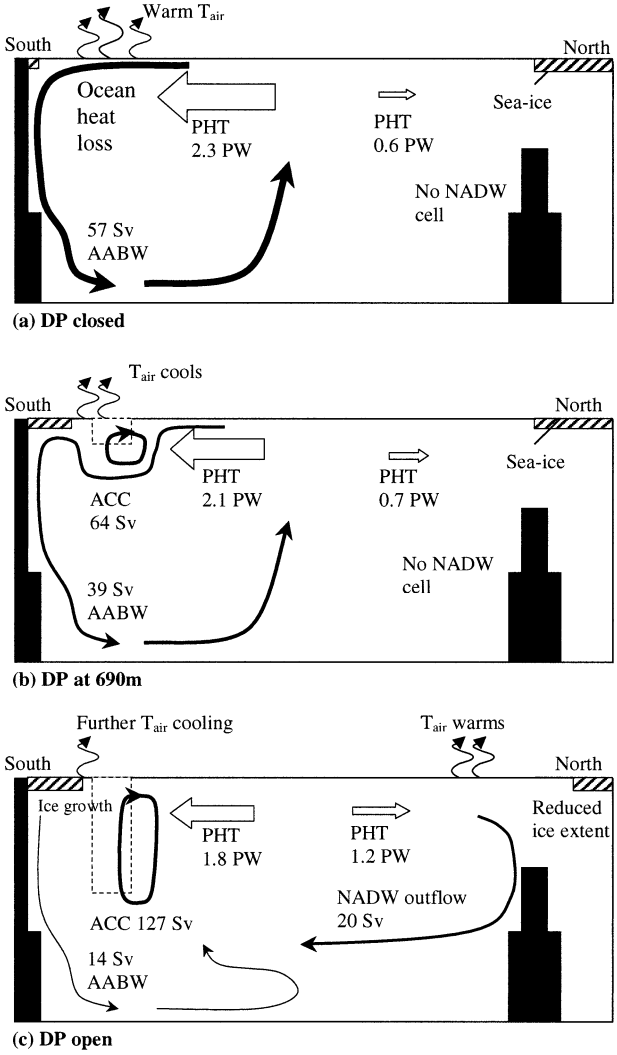

FIG. 9. Schematic representation of the major ocean circulation, heat transport, ice, and air temperature features of the three experiments.

restoring conditions for temperature and salinity, thus allowing both feedbacks 1 and 2 to operate.

The coupled model positive salt feedback and the self-stabilizing thermal feedback are the primary reasons for differences between our study and uncoupled models such as Nong et al. (2000). However, the wind feedback introduces small modifications as well, particularly in the SH. Comparing our DP_{clsd} results with the same run but with the wind feedback suppressed, we find that the ''east wind drift'' is reduced by approximately 10 Sv in the Weddell Sea and the Brazil Current is 4 Sv weaker in the wind feedback experiment. In contrast, the wind feedback does not have a significant effect on NH circulation (differenced streamfunction values are less than 2 Sv). This implies that the 20 Sv increase in Gulf Stream transport when DP is opened is almost exclusively the result of thermohaline effects. Although the wind feedback is an important component of the model, the thermal and salt feedback effects dominate in our experiments.

7. Discussion and conclusions

Our model results show how significant large-scale cooling of the Southern Hemisphere occurs when the Southern Ocean gateway is opened. The cooling is primarily driven by decreased poleward heat transport to the south, increased sea ice extent, and a subsequent increase in the sea ice albedo. This is contrasted by a warming in the Northern Hemisphere caused by NADW formation in the DP_{open} experiment, a process absent in the DP_{clsd} and DP_{690} experiments. The described changes when opening and deepening DP are summarized in a schematic in Fig. 9.

One of the key findings of our climate model study is that the Southern Hemisphere climate in DP_{690} is similar to that of DP_{open}, whereas the Northern Hemisphere climate in DP_{690} is similar to that of DP_{clsd}. This is because NADW is only initiated once the DP sill is sufficiently deep, whereas AABW production is reduced substantially once a shallow DP gateway is established. This suggests that any change in southern climate might have occurred rather abruptly upon DP opening during the Oligocene period, whereas a northern climate response was delayed until a deep gateway was formed.

The maximum of 15°C SAT cooling in May–July is

observed in the area between the Ross Sea and the Antarctic Peninsula. The maximum SAT difference is not located in this area during summer. Instead, it is located in the South Atlantic Brazil Current region near 50°S, showing a 6°C cooling. Important, the fact that the 15°C maximum area of SAT cooling is virtually absent in summer suggests a wintertime process, such as sea ice formation, is fundamentally different between the DP_{clsd} and DP_{open} experiments. This is confirmed in our sea ice analysis of section 4. Indeed, the wintertime surface air temperature difference maximum occurs in an area that is ice covered during winter in the DP_{open} experiment but is ice free year-round in the DP_{clsd} experiment. Warming in the Southern Hemisphere upon opening DP occurs south of Australia. SAT warming in this area is also seasonal because of increased sea ice frequency in the region.

It should be noted that the versions of the three main experiments presented here were rerun using the Gent and McWilliams (1990, hereinafter GM) eddy advection scheme. The GM experiments yield similar results to those presented here. This suggests that our findings are robust with respect to the choice of lateral eddy parameterization. SST differences between the model experiments are significantly smaller than SAT changes. This is because of the large capacity of seawater to store and release heat, which diminishes the sensitivity of SST to model geometry compared to that of SAT. Northward oceanic heat transport increases in both hemispheres for the DP_{open} experiment, reflecting both the onset of NADW formation and the lack of any significant geostrophic flow across the DP latitudes when an open gateway exists.

Southern Ocean sea ice extent for the DP_{open} experiment is significantly more than in the DP_{clsd} experiment except for the region northwest of the Ross Sea. It is the year-round absence of sea ice for DP_{clsd} in the regions west of the Antarctic Peninsula that causes the SAT differences to be largest (up to 15°C cooling in DP_{open} during winter). This is due to the insulating effect of ice and the resulting decrease in ocean–atmosphere heat loss when opening DP.

The SAT cooling across experiments is smallest in summer, although it is still significant (up to 4°C regionally). Summer temperatures are critical for determining whether an ice cap can build up on Antarctica, because the amount of snow and ice that survives the summer drives the buildup process, regardless of winter temperatures. Our results suggest that changes in ocean currents due to the opening of DP may have helped to contribute to the glaciation of Antarctica.

Acknowledgments. The authors are grateful to the University of Victoria, Andrew Weaver, and Michael Eby for supplying us with the Earth System Climate Model and invaluable technical and scientific advice regarding its use. They are also gratefully acknowledged for hosting a visit by Willem Sijp to the University of Victoria in May–June 2002. We also thank Oleg Saenko and Matthew Huber for valuable feedback and suggestions regarding the content of this paper. This research was supported by the Australian Research Council.

REFERENCES

Barker, P. F., and J. Burrell, 1977: The opening of Drake Passage. *Mar. Geol.,* **25,** 15–34.

Bryan, K., and L. J. Lewis, 1979: A water mass model of the World Ocean. *J. Geophys. Res.,* **84** (C5), 2503–2517.

——, S. Manabe, and M. J. Spelman, 1988: Interhemispheric asymmetry in the transient response of a coupled ocean–atmosphere model to a CO_2 forcing. *J. Phys. Oceanogr.,* **18,** 851–867.

Cox, M. D., 1989: An idealized model of the World Ocean. Part I: The global-scale water masses. *J. Phys. Oceanogr.,* **19,** 1730–1752.

Duffy, P. B., and K. Caldeira, 1997: Sensitivity of simulated salinity in a three dimensional ocean model to upper-ocean transport of salt from sea-ice formation. *Geophys. Res. Lett.,* **24,** 1323–1326.

England, M. H., 1992: On the formation of Antarctic Intermediate and Bottom Water in ocean general circulation models. *J. Phys. Oceanogr.,* **22,** 918–926.

——, 1993: Representing the global-scale water masses in ocean general circulation models. *J. Phys. Oceanogr.,* **23,** 1523–1552.

Fanning, A. F., and A. J. Weaver, 1996: An atmospheric energy–moisture balance model: Climatology, interpentadal climate change, and coupling to an OGCM. *J. Geophys. Res.,* **101,** 15 111–15 128.

Gent, P. R., and J. C. McWilliams, 1990: Isopycnal mixing in ocean general circulation models. *J. Phys. Oceanogr.,* **20,** 150–155.

Gill, A. E., and K. Bryan, 1971: Effects of geometry on the circulation of a three dimensional hemisphere ocean model. *Deep-Sea Res.,* **18,** 685–721.

Huber, M., L. Sloan, and C. Shellito, 2003: Early Paleogene oceans and climate: A fully coupled modeling approach using the NCAR CCSM. Geological Society of America Special Paper 369, 634 pp.

Hughes, T. M. C., and A. J. Weaver, 1994: Multiple equilibria of an asymmetric two-basin ocean model. *J. Phys. Oceanogr.,* **24,** 619–637.

Hunke, E. C., and J. K. Dukowicz, 1997: An elastic–viscous–plastic model for sea ice dynamics. *J. Phys. Oceanogr.,* **27,** 1849–1867.

Kalnay, E., and Coauthors, 1996: The NCEP/NCAR 40-Year Reanalysis Project. *Bull. Amer. Meteor. Soc.,* **77,** 437–471.

Kennett, J. P., 1977: Cenozoic evolution of Antarctic glaciation, the Circum Antarctic Ocean, and their impact on global paleoceanography. *J. Geophys. Res.,* **82,** 3843–3860.

Manabe, S., and R. J. Stouffer, 1988: Two stable equilibria of a coupled ocean–atmosphere model. *J. Climate,* **1,** 841–866.

Mikolajewicz, U., E. Maier-Reimer, T. J. Crowley, and K.-Y. Kim, 1993: Effect of Drake Passage and Panamanian gateways on the circulation of an ocean model. *Paleoceanography,* **8,** 409–426.

Nong, G. T., R. G. Najjar, D. Seidov, and W. H. Peterson, 2000: Simulation of ocean temperature change due to the opening of Drake Passage. *Geophys. Res. Lett.,* **27,** 2689–2692.

Pacanowski, R., 1995: MOM 2 documentation user's guide and reference manual. GFDL Ocean Group Tech. Rep. 3, GFDL, Princeton, NJ, 329 pp.

Rahmstorf, S., 1996: On the freshwater forcing and transport of the Atlantic thermohaline circulation. *Climate Dyn.,* **12,** 799–811.

——, and J. Willebrand, 1995: The role of temperature feedback in stabilizing the thermohaline circulation. *J. Phys. Oceanogr.,* **25,** 787–805.

——, and M. H. England, 1997: On the influence of Southern Hemisphere winds on North Atlantic Deep Water flow. *J. Phys. Oceanogr.,* **27,** 2040–2054.

Saenko, O. A., J. M. Gregory, A. J. Weaver, and M. Eby, 2002: Distinguishing the influences of heat, freshwater and momentum

fluxes on ocean circulation and climate. *J. Climate,* **15,** 3686–3697.

Toggweiler, J. R., and B. Samuels, 1995: Effect of Drake Passage on the global thermohaline circulation. *Deep-Sea Res.,* **42A,** 477–500.

——, and H. Bjornsson, 2000: Drake Passage and paleoclimate. *J. Quat. Sci.,* **15,** 319–328.

Weaver, A. J., and Coauthors, 2001: The UVic Earth System Climate Model: Model description, climatology, and applications to past, present and future climates. *Atmos.–Ocean,* **39,** 361–428.

Zang, S., R. J. Creatbatch, and C. A. Lin, 1993: A reexamination of the polar halocline catastrophe and implications for coupled ocean–atmosphere modeling. *J. Phys. Oceanogr.,* **23,** 287–299.